PNAS RESEARCH ARTICLE | NEUROSCIENCE

Examining the role of dopamine in methylphenidate's effects on resting brain function

Dardo Tomasi[a,1], Peter Manza[a], Weizheng Yan[a], Ehsan Shokri-Kojori[a], Şükrü Barış Demiral[a], Michele-Vera Yonga[a], Katherine McPherson[a], Catherine Biesecker[a], Evan Dennis[a], Allison Johnson[a], Rui Zhang[a], Gene-Jack Wang[a], and Nora D. Volkow[a]

Edited by Donald Pfaff, Rockefeller University, New York, NY; received August 23, 2023; accepted November 14, 2023

The amplitude of low-frequency fluctuations (ALFF) and global functional connectivity density (gFCD) are fMRI (Functional MRI) metrics widely used to assess resting brain function. However, their differential sensitivity to stimulant-induced dopamine (DA) increases, including the rate of DA rise and the relationship between them, have not been investigated. Here we used, simultaneous PET-fMRI to examine the association between dynamic changes in striatal DA and brain activity as assessed by ALFF and gFCD, following placebo, intravenous (IV), or oral methylphenidate (MP) administration, using a within-subject double-blind placebo-controlled design. In putamen, MP significantly reduced $D_{2/3}$ receptor availability and strongly reduced ALFF and increased gFCD in the brain for IV-MP (Cohen's d > 1.6) but less so for oral-MP (Cohen's d < 0.6). Enhanced gFCD was associated with both the level and the rate of striatal DA increases, whereas decreased ALFF was only associated with the level of DA increases. These findings suggest distinct representations of neurovascular activation with ALFF and gFCD by stimulant-induced DA increases with differential sensitivity to the rate and the level of DA increases. We also observed an inverse association between gFCD and ALFF that was markedly enhanced during IV-MP, which could reflect an increased contribution from MP's vasoactive properties.

simultaneous PET/MRI | methylphenidate | dopamine | functional connectivity | spontaneous brain activity

Significance

Stimulant medications are safe and effective for the treatment of attention-deficit-hyperactivity disorder (ADHD) but they can also have rewarding effects when injected. We employed cutting-edge simultaneous positron emission tomography (PET) and functional magnetic resonance imaging (fMRI) to investigate the association between dynamic changes in striatal dopamine (DA) and brain activity measured by the amplitude of low-frequency fluctuations (ALFF) and global functional connectivity density (gFCD). MP (methylphenidate) resulted in increased DA levels, accompanied by significant reductions in ALFF and increases in gFCD. Notably, the effect was much more pronounced for IV (intravenous)-MP, with changes of up to 100%, compared to oral-MP, with changes of less than 10%. These findings shed light on the distinct sensitivity of ALFF and gFCD to neuronal activation, with implications for the differential vasoactive contribution to these metrics.

Methylphenidate (MP) is a stimulant drug currently used to treat attention-deficit hyperactivity disorder (ADHD) symptomatology in ~10% of school-aged children (1). The rise in the medical use of stimulant drugs among school-aged children has coincided with an increase in nonmedical use, particularly in schools with high rates of medical usage (2). Additionally, a significant number of individuals without an ADHD diagnosis either receive stimulants due to improper diagnoses or misuse them, often seeking the rewarding or perceived cognitive-enhancing effects (3). While oral MP is generally considered safe for ADHD treatment, when injected, MP also has rewarding effects, which can lead to addiction (4).

Functional MRI (fMRI) studies have advanced our understanding of the effects of psychoactive drugs in the human brain including that of stimulant medications (5, 6). Resting-state fMRI metrics have emerged as valuable tools for investigating the effects of stimulant drugs on brain activity in various populations (7–12). For instance, the amplitude of low-frequency fluctuations (ALFF), a metric that quantifies the intensity of spontaneous low-frequency oscillations in the fMRI signal during rest and provides insights into baseline brain activity (13), has been used to assess the effects of stimulant drugs in healthy controls and participants with ADHD (14, 15). Among these are studies of the effect MP on the spontaneous low-frequency fluctuations of the fMRI signals that give rise to brain functional connectivity (16). Resting-state functional connectivity (rsFC) studies in healthy controls and participants with ADHD have been used to assess the effects of MP in brain connectivity, particularly in frontostriatal circuitry though findings have been inconsistent with some studies showing increases and other decreases in connectivity [(reviewed in Birn et al. (17)]. Although a couple of studies have examined the associations between ALFF and other rsFC metrics (18, 19), to the best of our knowledge, no investigation has explored such associations under the influence of a stimulant medication. Additionally, to our knowledge, there are no published human studies on the effects of acute MP administration on ALFF. Furthermore, our understanding of the modulation of ALFF vs. other rsFC metrics by DA (dopamine) and its dynamics remains very limited.

The advent of PET/MRI scanners capable of simultaneous imaging of molecular radiotracers with PET and blood-oxygen-level-dependent (BOLD) signals with fMRI has provided a unique opportunity to investigate the real-time interactions between neurotransmitter

Author contributions: D.T. and N.D.V. designed research; D.T., P.M., M.-V.Y., K.M., C.B., E.D., A.J., and G.-J.W. performed research; D.T. contributed new reagents/analytic tools; D.T., P.M., W.Y., E.S.-K., Ş.B.D., and R.Z. analyzed data; and D.T. and N.D.V. wrote the paper.

The authors declare no competing interest.

This article is a PNAS Direct Submission.

[1]To whom correspondence may be addressed. Email: dardo.tomasi@nih.gov.

This article contains supporting information online at https://www.pnas.org/lookup/suppl/doi:10.1073/pnas.2314596120/-/DCSupplemental.

Published December 18, 2023.

signaling and brain activation patterns (20). This groundbreaking technology demonstrated its potential in elucidating the relationship between DA signaling and brain activation patterns in nonhuman primates. Specifically, in anesthetized monkeys increasing doses of the $D_{2/3}$ receptor antagonist raclopride were associated with proportional increases in cerebral blood volume [an indirect marker of cerebral activity (21)]. These effects were concurrent with decreases in [11C]raclopride striatal binding due to direct receptor blockade by the pharmacological doses of raclopride (22, 23). In awake monkeys increasing doses of MP reduced [^{18}F]fallypride striatal binding (reflecting DA increases triggered by oral MP) which was proportionally linked to increased rsFC between the caudate and dorsolateral prefrontal cortex (PFC), precuneus, and hippocampus (17). However, despite these promising findings in nonhuman primates, the application of this methodology in humans remains largely unexplored. Here, we leverage the simultaneous PET/MRI approach to investigate how dynamic changes in striatal DA induced by MP influence ALFF and rsFC metrics.

In this study, we utilized cutting-edge simultaneous [11C]raclopride PET-fMRI to investigate and compare the dynamic changes in DA levels in the striatum. To comprehensively assess brain activity and connectivity, we examined the dynamics of ALFF and of global functional connectivity density (gFCD) (24). ALFF provides insights into the strength of spontaneous brain fluctuations (13), while gFCD serves as a marker of centrality and brain energy demand (25). By integrating these advanced imaging techniques, we aimed to gain a more comprehensive understanding of the neurobiological effects of DA and its potential implications for brain function. We contrasted oral-MP, which leads to gradual DA increases, and IV (intravenous)-MP, which results in fast DA increases (26) with oral and IV placebo (PL) administrations, in a cohort of 20 healthy adults. For equivalency, we selected doses of 60 mg oral MP and 0.25 mg/kg IV-MP, which we had previously shown led to similar levels of DA transporter (DAT) occupancies (27), the target by which MP increases DA, employing a double-blind, placebo-controlled, within-subject design. Each participant underwent three separate sessions on different days, with the order of administration counterbalanced across participants (*SI Appendix*, Fig. S1*A*).

Results

The dataset utilized in this study consisted of 90-min simultaneous PET-fMRI scans obtained from 20 healthy individuals. The scans were acquired during three separate sessions, PL, oral-MP, and IV-MP, which were randomly ordered for each participant. The scans were conducted under resting conditions, with MP serving as the pharmacological challenge. As depicted in *SI Appendix*, Fig. S1, each session commenced with the administration of an oral pill (either 60 mg MP or PL) 30 min before the injection of [^{11}C]raclopride, a DA D2/3 receptor ligand sensitive to DA competition for its binding (28). The PET/MRI data acquisition commenced at the time of the tracer injection and was followed 30 min later by IV injection (either 0.25 mg/kg MP or PL). We timed the pharmacological challenges to ensure that both oral-MP and IV-MP resulted in similar time-to-peak concentrations of MP in the striatum as derived from the brain pharmacokinetics findings of previous PET studies with [^{11}C]MP (4, 29). The DA increase and rate induced by MP were estimated from ΔSUVr(t), the time-varying standardized uptake values [relative to the cerebellum (cer)] computed using the difference between the PL and MP conditions (26).

MP Decreased Striatal $D_{2/3}$ Receptor Availability: DA Increases. To assess changes in $D_{2/3}$ receptor availability, we estimated the nondisplaceable binding potential (BPnd) of [^{11}C]raclopride using a graphical analysis that does not require blood sampling with the cer as the reference region (30). We previously reported that BPnd values were significantly lower for both IV- and oral-MP compared to PL, demonstrating substantial DA increases in the striatum throughout the 90-min scans ($P_{FWE} < 0.05$, family-wise error corrected at the cluster-level; *SI Appendix*, Fig. S1*B*) (26).

MP blocks the DAT (27), leading to increases in extracellular DA (31) that compete for binding to $D_{2/3}$ receptors with [^{11}C]raclopride (28). In our prior work, we estimated time-varying DA increases in the striatum (putamen, caudate, and ventral striatum) by contrasting the time courses of striatal SUVr between PL and MP conditions (26). The SUVr difference (ΔSUVr) in striatal regions between PL and MP conditions (IV and oral) reflected increases in endogenous DA (*SI Appendix*, Fig. S1*C*). The average of these differences across participants was accurately modeled by gamma cumulative distribution functions ($R^2 > 0.95$), representing the accumulation of synaptic DA. Findings in the stiatal regions were similar but had more variability in caudate and ventral striatum than in putamen; so for subsequent analyses of DA dynamics, we focused on putamen.

Frequency Domain Dynamics: Effect of IV- and Oral-MP. IV-MP caused a pronounced drop in the whole brain fMRI signal that was more prominent during the first 20 min after injection (30 < t < 50 min; early MP-response period) followed by a gradual but incomplete recovery over time (50 < t < 90 min; late MP-response period). To study the dynamics and spectral characteristics of these changes following MP administration we conducted a spectral analysis of the fMRI signal. The average reduction in z-scored Fourier amplitudes after baseline subtraction was significantly larger for IV-MP compared to both oral-MP and PL in all frequency bins within the 0.02 to 0.16 Hz band, for the early and late MP-response periods ($P < 0.004$, FDR (false discovery rate)-corrected; 2-sided paired t test; Fig. 1*A*). Within the 0.02 to 0.16 Hz band the reductions were greater for the slowest frequencies (0.02 to 0.10 Hz). There were no significant differences between oral-MP and PL conditions.

We examined the effects of oral-MP and IV-MP on the dynamics of ALFF in the traditional 0.01 to 0.10 Hz low-frequency band with a standard sliding window approach at a temporal resolution of 1 min to assess the dynamic changes. The whole-brain average values of ALFF(t) showed a decrease of 20 to 50% following IV-MP injection (30 < t < 90 min; t > 24.2, df = 1,626, $P <$ 2E-16, linear mixed-effects model) compared to the baseline period (0 < t < 30 min). Much smaller decreases were observed during oral-MP (5 to 10%, t > 5.4, df = 1,612, P<8E-08; Linear mixed-effects model), but not during PL ($P > 0.3$).

Dynamic Associations between ALFF and DA Increases. Since fast (phasic) DA increases would activate both stimulatory, low-affinity D1 receptors and inhibitory high-affinity D2 receptors, while slow (tonic) DA increases would predominantly activate only D2 receptors (32), we hypothesized that changes in DA levels triggered by oral- and IV-MP would distinctly affect the fMRI signal in the basal ganglia and cortical regions where DA receptors are located and also in the regions to which they project (33). To assess the effects of DA increases on ALFF we conducted a within-subject multilinear regression analysis. The average time courses across the 20 participants and 91,282 grayordinates revealed marked reductions in ALFF(t) after IV-MP injection that were explained by the average DA increases across participants in putamen ($R^2 > 0.96$, $P <$ 2E-16). Specifically, we used a gamma cumulative distribution function, $F(t)$, to fit the time-varying PET signal that reflected the time-varying DA changing level (or "amplitude")

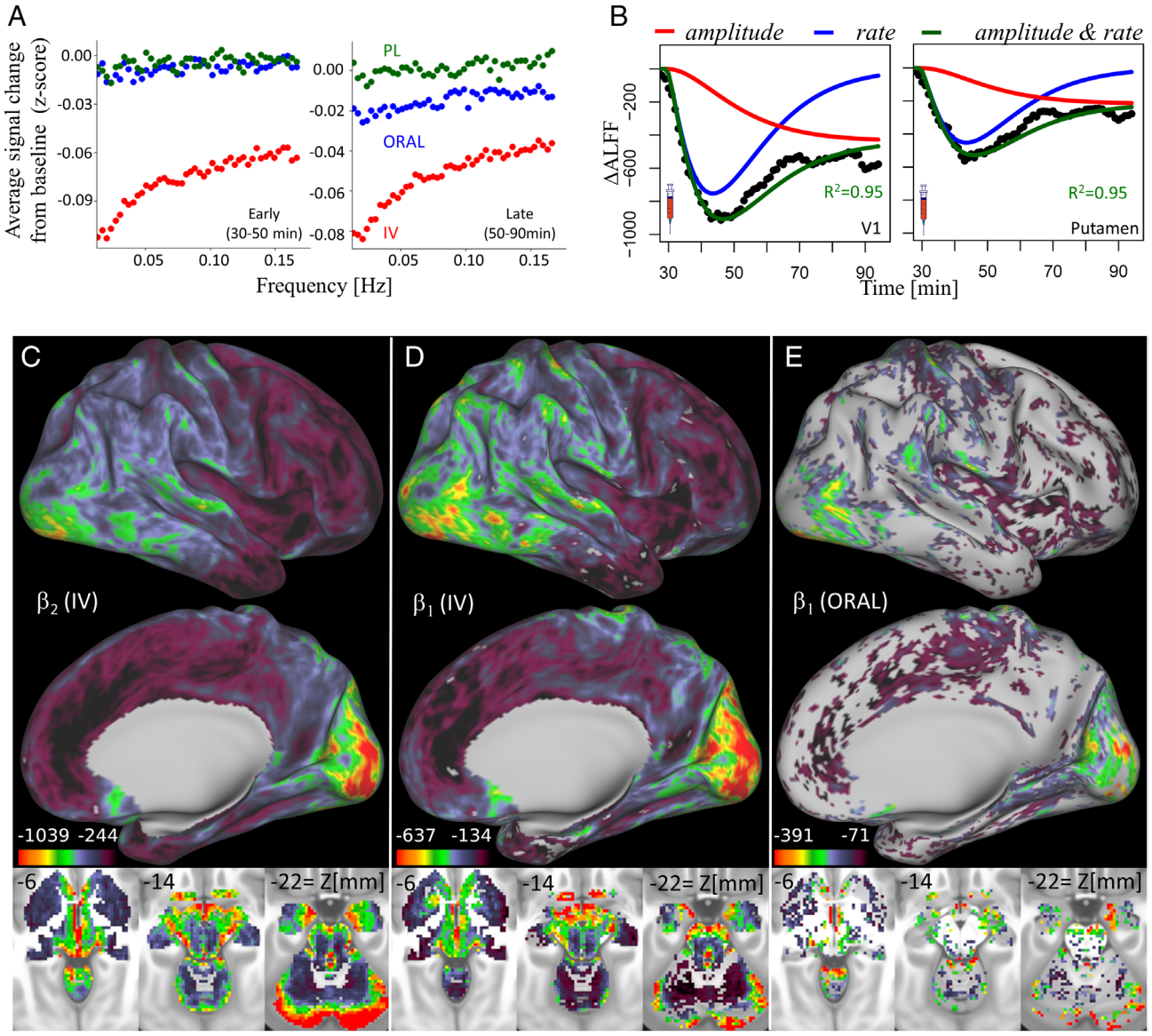

Fig. 1. Decreases in ALFF induced by MP. (*A*) Average frequency domain changes in the whole-brain fMRI signal, compared to the baseline period (5 < t < 30 min), for the early (30 < t < 50 min; *Left*) and late (50 < t < 90 min; *Right*) posttracer injection periods across 20 healthy adults for PL, IV-, and oral-MP. (*B*) Dynamics of the ALFF after baseline subtraction (ΔALFF) in bilateral putamen and primary visual cortex (V1) for IV-MP. The curves represent estimated time courses derived from the amplitude and rate of DA increases using Eq. **1**. (*C–E*) Average slopes of the linear associations of the ALFF with $f(t)$ ("dopamine rate"; β_2; *C*) and $F(t)$ ("dopamine amplitude"; β_1; *D* and *E*) overlaid on inflated lateral (*Top*) and medial (*Middle*) surfaces of the right human brain hemisphere and on 3 axial views showing the subcortical brain regions (*Bottom*) using a FDR threshold $P_{FDR} < 0.05$, for IV and oral MP. Sample size: 20 healthy adults. 2-sided *t* test.

induced by MP in the putamen. We also calculated $f(t)$, a gamma probability density function reflecting the speed (or "rate") of DA changes over time, by taking the derivative of $F(t)$. These dynamic variables were then used to model the ALFF changes induced by MP using the bilinear model: $ALFF(\boldsymbol{x}, t) \sim \beta_1(\boldsymbol{x})\ F(t) + \beta_2(\boldsymbol{x})\ f(t)$. Fig. 1 shows that the rate component reflects more transient changes in DA, whereas the amplitude component captures both transient and longer-term alterations. The bilinear model also captured the average MP-related decreases in ALFF following oral-MP ($0.19 < R^2 < 0.3$; $P < 0.003$, Bonferroni corrected), but not those after PL ($P > 0.06$). During IV-MP, the dynamics of ALFF(t) were significantly coupled to $f(t)$ in most cortical and subcortical partitions (β_2), including the putamen and the primary visual cortex (V1) regions-of-interest (ROIs) (Fig. 1*B*).

Using a vertex-wise *t* test on β_1, the slope of the association with $F(t)$, we observed a predominant effect of the amplitude of DA increases on ALFF(t) in subcortical regions (sc) (medial and posterior thalamic nuclei, midbrain, hypothalamus, basal nucleus of Meynert, ventral amygdala, and ventral striatum) and the occipital cortex, both for IV- and oral-MP conditions [$P_{FDR} < 0.05$; 0.7 < Cohen's d < 1.6 (oral) or 1.9 (IV); Fig. 1].

Similarly, the slope of the association with $f(t)$, β_2, demonstrated a pronounced effect of the rate of DA increases on ALFF(t) in the same sc and for most cortical regions during IV-MP ($P_{FDR} < 0.05$; 0.7 < Cohen's d < 2; Fig. 1) but not for oral-MP. Insula, anterior, and posterior cingulate cortices, and temporal pole exhibited higher β_2 for IV- than oral-MP ($P_{FDR} < 0.05$; 0.7 < Cohen's d < 1.3).

In the case of ALFF during IV-MP, the average slopes of the bilinear model (β_1 and β_2) were significantly negative within the cer, sc, and each of 12 resting state networks (34) (RSN; $P < 0.01$; Fig. 2*A*), indicating that MP-related DA increases were associated with decreased ALFF. For oral-MP, the average β_1 within these partitions also showed significant negative values ($P < 0.02$; Fig. 2*B*), while β_2 was not significant.

Association between gFCD and the Rate of DA Increases. The whole-brain average values of gFCD(t) increased after IV-MP injection (30 < t < 60 min; t = 11.7, df = 1,626, P <2E-16, Cohen's d = 1.5, linear mixed-effects model; Fig. 3*A*), compared to the baseline (0 < t < 30 min), but there was no significant difference between these time windows for oral-MP nor for PL (P > 0.2). The average gFCD time courses across participants and grayordinates demonstrated significant increases after IV-MP injection, which were primarily explained by the rate of DA increases.

In sc (nucleus accumbens, putamen, caudate, pallidum, thalamus, amygdala, hippocampus, midbrain, and the cer), but not in cortical regions, the slope of the linear association between gFCD and the rate of DA increases (β_2) was stronger for IV- than oral-MP (P < 0.03; Fig. 3*B*). During IV-MP, the linear association between the rate of DA increases and gFCD(t) was strongest in the putamen, posterior thalamus, and anterior cer lobe and moderate in nucleus accumbens, caudate, PFC, insula, and parahippocampal gyrus (P_{FDR} < 0.05; 0.7< Cohen's d < 1.6; Fig. 3 *C* and *D*). The linear association between $F(t)$ and gFCD was not significant.

In the case of gFCD, the average slopes of the bilinear model (β_1 and β_2) were significantly positive within the cer, sc, and the 12 RSN during IV-MP (P < 1E-04; Fig. 3 *D* and *E*). During oral-MP, the average β_1 and β_2 were not significant.

Association between ALFF and gFCD. Across individuals, ALFF and gFCD demonstrated a significant positive temporal correlation in occipital and parietal cortices during oral-MP (P_{FDR} < 0.05; Fig. 4*A*) and PL conditions (*SI Appendix*, Fig. S2). However, during IV-MP, there was a strong negative correlation observed in the remaining brain regions (Fig. 4*B*). Notably, in the putamen, the average dynamics of ALFF and gFCD exhibited a negative correlation during IV-MP (R = −0.96), indicating that time windows with the largest gFCD increases coincided with ALFF decreases. Nevertheless, these correlations were notably weaker for PL (R = −0.4) and oral-MP (R = −0.51) compared to IV-MP (Fig. 4*C*). Cortical ROIs that showed higher coupling of DA levels with ALFF had higher coupling with gFCD, independently for IV- and oral-MP, and for β_1 and β_2 (R(358) > 0.72; P < 2E-16). Similarly for IV-MP, subcortical ROIs that demonstrated higher coupling of DA levels with ALFF had higher coupling with gFCD, independently for β_1 and β_2 (R(17) > 0.77; P < 1E-04; *SI Appendix*, Fig. S3); however, for oral-MP, this association was verified for β_1 (R(17) = 0.67; P < 0.002) but not for β_2.

Cardiovascular Effects. Using linear mixed-effects modeling, we found that $F(t)$ and $f(t)$ were predictors of heart rate and systolic blood pressure [t > 2.0, P < 0.05]. MP increased all 3 cardiovascular metrics compared to PL [F(2, 1,816) > 5.0; P < 0.007]. Similarly, heart rate and systolic and diastolic blood pressures were predictors of gFCD(t) and ALFF(t) (|t| > 3.5, P < 6E-04).

Discussion

In this study, we employed simultaneous PET-fMRI with IV- and oral-MP to explore differences in ALFF and gFCD based on the amplitude and rate of DA increases induced by MP. Our findings revealed that DA increases in the putamen were associated with concurrent decreases in ALFF, which predominated in the vicinity

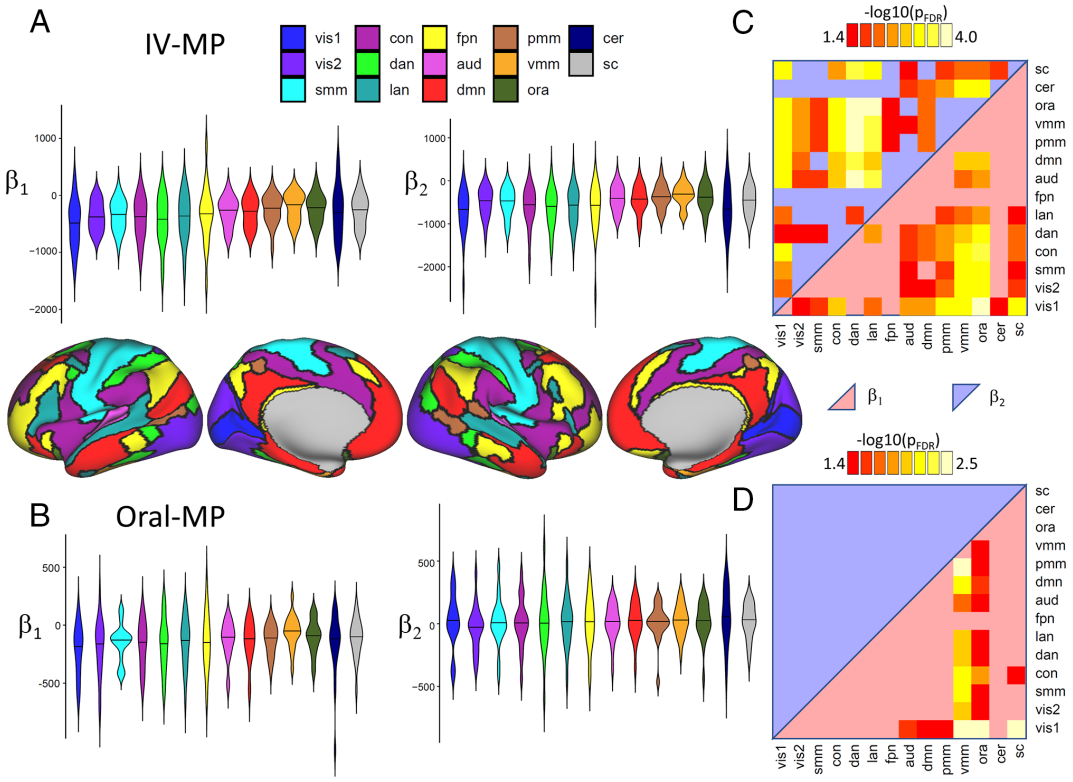

Fig. 2. Neurovascular coupling: Network analysis. The slopes of the bilinear model representing the associations between the ALFF and the amplitude (β_1) and rate (β_2) of DA increases elicited by IV and oral MP are shown. These average slopes are shown for 12 RSN, subcortical, and cerebellar regions. Statistical comparisons within networks across vertices were performed for β_1 and β_2, separately for IV-MP (*A*) and oral-MP (*B*), and between-network differences in β_1 and β_2, independently for IV-MP (*C*) and oral-MP (*D*). The partitions include primary and secondary visual (vis), somatomotor (smm), cingulo-opercular (con), dorsal attention (dan), language (lan), frontoparietal (fpn), auditory (aud), default-mode (dmn), posterior multimodal (pmm), ventral multimodal (vmm), orbito-affective (ora), subcortical (sc), and cerebellum (cer) regions. Statistical analysis: 2-sided paired t test with a significance threshold of PFDR < 0.05, FDR corrected for multiple comparisons. The data were derived from a cohort of 20 healthy adults.

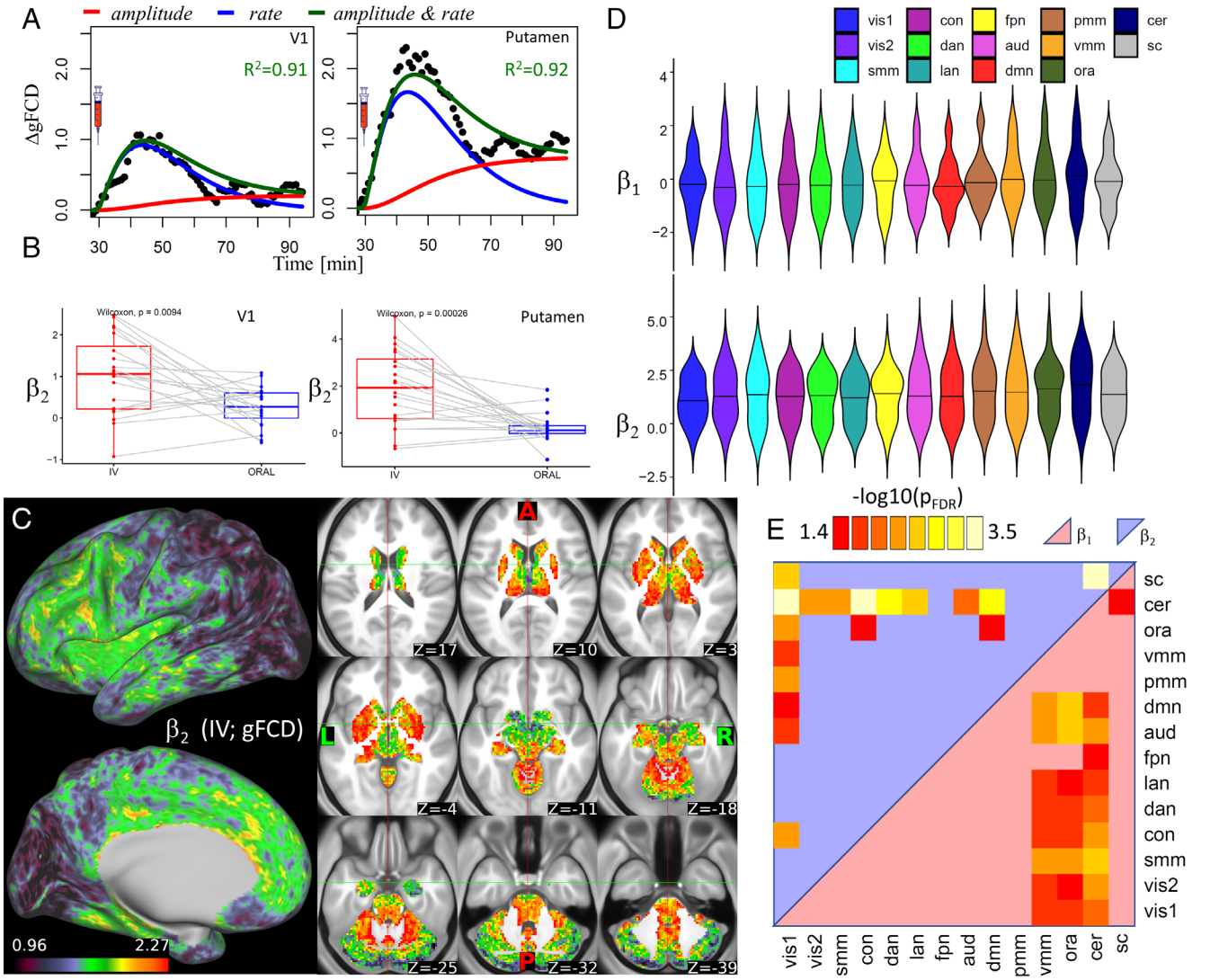

Fig. 3. Coupling between DA rate and gFCD (β_2). (*A*) Average time courses across 20 healthy adults showing the changes in dynamic gFCD after baseline subtraction (ΔgFCD) in the primary visual cortex (V1) and the putamen; the curves represent estimated time courses derived from the amplitude and rate of DA increases in putamen elicited by IV-MP using Eq. **1**. (*B*) Paired plots showing β_2 differences between IV- and oral-MP in V1 and the putamen. (*C*) Average β_2 overlaid on inflated lateral (*Top*) and medial (*Bottom*) surfaces of the left human brain hemisphere and on 9 axial views of subcortical and cerebellar regions using a FDR threshold $P_{FDR} < 0.05$. (*D*) Slopes of the associations between gFCD and the amplitude (β_1) and rate (β_2) of DA increases elicited by IV-MP, averaged within 12 RSN, subcortical, and cerebellar regions. (*E*) Statistics of between-network differences in β_2 for IV-MP. The partitions include primary and secondary visual (vis), somatomotor (smm), cingulo-opercular (con), dorsal attention (dan), language (lan), frontoparietal (fpn), auditory (aud), default-mode (dmn), posterior multimodal (pmm), ventral multimodal (vmm), orbito-affective (ora), subcortical (sc), and cerebellum (cer) regions. Statistical analysis: 2-sided *t* test with a significance threshold of $P_{FDR} < 0.05$, FDR corrected for multiple comparisons. The data were derived from a cohort of 20 healthy adults.

of the Circle of Willis, the transverse sinus, and primary visual cortex, and with concomitant increases in gFCD that predominated in striatum, thalamus, amygdala, parahippocampal gyrus, anterior cer, PFC, and insula and were more pronounced for IV-MP compared to oral-MP in sc and cer.

The dynamic spectral analysis revealed a significant reduction in fMRI signal fluctuations immediately following IV-MP administration, particularly at lower frequencies. The reduction in ALFF could reflect the arousing and wakefulness-promoting effects of stimulant drugs like MP (35) since when arousal levels are low, as is the case during nonrapid eye movement sleep, the amplitude of the low-frequency components of the fMRI signal is high compared to wakefulness (36). Similarly in nonhuman primates, behavioral arousal has been linked to reductions in fMRI signal amplitude in cortical regions, though in sc it was linked with signal increases (37). In humans, decreased arousal as the day progresses was shown to increase global signal amplitude while reducing rsFC (38). This suggests that MP-induced increases in arousal contributes to the observed decrease in fMRI signal fluctuations at low frequencies and to the gFCD increase.

The observed decrease in ALFF with IV-MP poses a challenge when attributing it solely to neuronal activity, as it contradicts the prior findings of increased brain glucose metabolism associated with IV-MP (39). Interestingly, the association between ALFF and gFCD was positive in the visual cortex during PL and oral-MP and negative in subcortical, cerebellar, and most cortical regions except for the visual cortex during IV-MP. The reversed direction of the association in cortical regions between oral-MP (and PL) compared to IV-MP, along with the similar but stronger negative association observed in putamen (and other sc), suggests that the neurovascular responses underlying the negative associations are intensified by IV-MP administration, highlighting a differential sensitivity of ALFF and gFCD to cerebrovascular reactivity (40). This is relevant because stimulant drugs particularly when injected have the

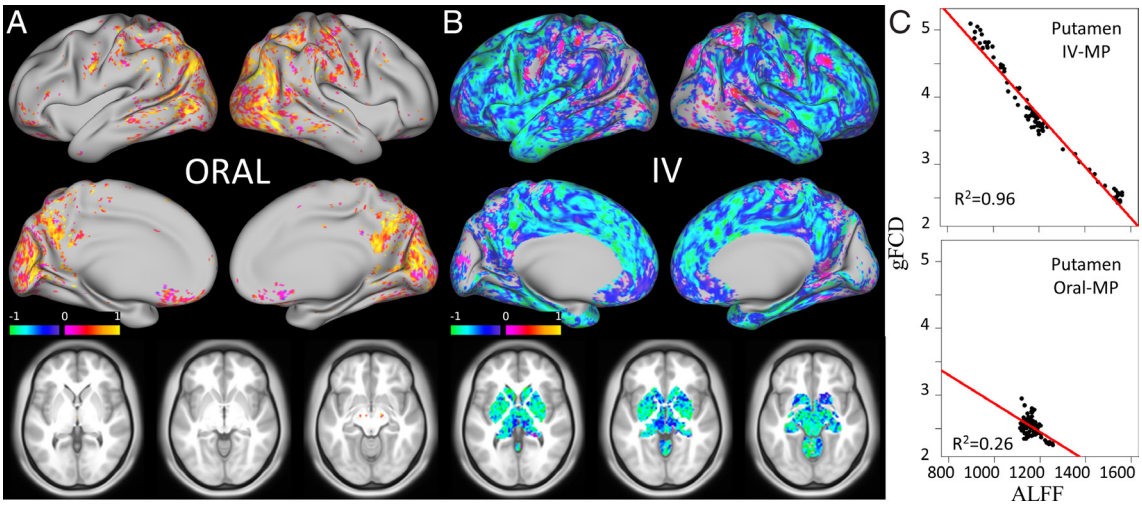

Fig. 4. Association between ALFF and gFCD. Fisher-z mean correlation between the ALFF dynamics and gFCD dynamics for oral (*A*) and IV (*B*) MP, overlaid on inflated lateral (*Top* row) and medial (*Middle* row) surfaces of the human brain, and on 3 axial views of subcortical and cerebellar regions (*Bottom* row) using a FDR threshold $P_{FDR} < 0.05$. Scatter plots showing the linear associations between time-varying ALFF and gFCD, averaged across individuals, for IV- and oral-MP (*C*); data points correspond to 85 time windows. Statistical analysis: 2-sided *t* test. The data were derived from a cohort of 20 healthy adults.

potential to induce cerebral vasoconstriction and disrupt neurovascular processes (41). In fact, our studies involving multimodal imaging in laboratory animals demonstrated that IV-cocaine, a pharmacologically similar stimulant drug to MP (42) caused vasoconstriction of cerebral blood vessels and reduced cerebral blood flow (CBF) (43) even though it increased neuronal activity (42). Consequently, vasoconstriction resulting from IV-MP could lead to a reduction in ALFF, similar to what has been reported in cases of hypocapnia, which also induces vasoconstriction (44). In this respect it's noteworthy that the regions that showed the most pronounced reductions in ALFF were located in the vicinities of the Circle of Willis at the base of the brain and of the transverse sinus that runs in the lateral border of the tentorium cerebelli and collects deoxygenated blood from draining veins in visual areas.

Intriguingly, the regions displaying the most significant reductions in ALFF are not usually regarded as primary DA targets. Conversely, the gFCD results exhibit a pattern that aligns more consistently with DA projections. However, the extent to which functional connectivity is insensitive to changes in blood vessel diameters in unclear, for early studies reported reduced resting-state fMRI signals and functional connectivity during prolonged hypercapnia (45), though more recent ones have shown that similar networks can be extracted during rest and hypercapnia periods (46). The marked gFCD increase in subcortical and anterior cortical regions in proportion to the rate of DA increases in putamen elicited by IV-MP is consistent with observations of enhanced striatal, pallidal, and frontal activation after stimulation of DA neurons in the ventral tegmental area (47, 48) as well as findings of associations between higher DA synthesis capacity and heightened brain activity and rsFC (49, 50) and with the role of DA in modulating rsFC (51).

While the observed positive associations between gFCD and ALFF during PL and oral-MP in posterior brain regions are supported by our prior work (52), the strong negative association between gFCD and ALFF during IV-MP was surprising, as this relationship has not been previously studied with stimulant drug administration. It also contradicted our expectations, as our previous research had shown that resting glucose metabolism was positively associated with both gFCD and ALFF (25). As for IV-MP, using PET we had documented distinct effects for metabolic vs. blood flow markers of brain activity. Specifically, IV-MP decreased whole-brain CBF (53) whereas it increased whole-brain glucose metabolism (39), a direct marker of neuronal activity. In those studies, the largest metabolic increases were in the thalamus and cer (39) which were regions where IV-MP increased functional connectivity (54). Therefore, the observed rise in gFCD seen with IV-MP and to a lesser degree with oral-MP, particularly in sc and cer, aligns with the notion that it represents heightened neuronal activation.

In our study, we observed distinct effects on ALFF and gFCD related to the rate and amplitude of DA increases following oral- and IV-MP administrations. We found that increased DA amplitude was associated with decreased ALFF, both for oral- and IV-MP and with increased gFCD for IV-MP. DA rate was also associated with decreased ALFF and increased gFCD during IV-MP but not during oral-MP. The association of DA rate and amplitude with the decreases in ALFF for IV-MP, which were in the opposite direction to the increase in gFCD, also raises the possibility of potential bidirectional associations between neuronal and vascular reactivity. While we hypothesize that fast (phasic) DA increases would activate both stimulatory, low-affinity D1 receptors and inhibitory high-affinity D2 receptors, we anticipate that slow (tonic) DA increases would predominantly activate D2 receptors. However, further research is needed to fully elucidate the underlying mechanisms responsible for these components. It's possible that the amplitude and rate components represent different phases of the signal change, with more rapid/transient changes associated with D1 receptor activation and prolonged changes potentially linked to longer-lasting D2 receptor activation.

A key limitation of this study is the relatively small sample size, which precluded the investigation of potential sex differences. Nonetheless, the robust magnitude of the changes induced by MP enabled us to obtain significant findings. When injected, stimulant drugs can directly influence the vascular system, altering CBF dynamics, which can impact fMRI signals and may have contributed to the observed decrease in signal fluctuations. We observed significant associations of MP-induced changes in cardiovascular function (heart rate and blood pressure) with the amplitude and rate of DA increases in the putamen, which is consistent with MP's ability to increase sympathetic nervous system activity leading to changes in heart rate and blood pressure (55). Therefore, alterations in sympathetic activity caused by MP could result in parallel changes in cardiovascular function and striatal DA dynamics.

In summary, our study employing simultaneous PET-fMRI revealed distinct dopaminergic modulation of brain activity in humans following fast (IV) and slow (oral) challenges with MP. Increases in striatal DA levels induced by MP administration were accompanied by a prominent reduction in ALFF at lower frequencies. Notably, IV-MP administration resulted in increased brain connectivity in basal ganglia regions, thalamus, anterior cer, and anterior cortices that were associated with the rate of DA increases. These findings show that MP promotes increased brain connectivity while reducing ALFF, which could reflect a combination of DA's neuronal and vascular effects. Our results also highlight the differential effects of fast and slow changes in DA signaling on brain activity.

Methods

Participants. A total of 20 healthy adults (mean age: 36.1 ± 9.6 y; 9 females) completed the study, undergoing scanning on three separate days with an average interval of 40 ± 35 d between sessions. The participants were exposed to different pharmacological conditions during each session: 1) oral administration of MP (60 mg) and IV administration of placebo (3 cc saline), 2) oral placebo and IV administration of MP (0.25 mg/kg in 3 cc sterile water), and 3) oral placebo and IV administration of placebo. The session order was randomized across participants, ensuring a double-blind and counterbalanced design in this placebo-controlled study. Both the participants and the researchers were unaware of the nature of the stimulant drug (MP/PL) during the study, further ensuring blinding throughout the experiment. All individuals provided informed consent to participate in this double-blind placebo-controlled study, which was approved by the IRB at the NIH (Combined Neurosciences White Panel; Protocol 17-AA-0178; ClinicalTrials.gov Identifier: NCT03326245)

Simultaneous PET/MRI Acquisition. Simultaneous PET/MRI imaging was conducted using a 3T Biograph mMR scanner (Siemens; Medical Solutions, Erlangen, Germany) equipped with a 12-channel head coil. PET and fMRI data were simultaneously acquired over a duration of 90 min, with timestamps allowing for post hoc data synchronization. The list mode PET data acquisition began 30 min after the oral administration of the pill, immediately following a manual injection of [^{11}C]raclopride as a bolus (dose =15.7 ± 1.9 mCi; duration 5 to 10 s). The fMRI data were continuously acquired, covering the entire brain, using a single-shot gradient-echo-planar imaging sequence (TR/TE = 3,000/30 ms; FA = 70 deg; matrix = 64, 36 axial slices; 4 mm thickness; 3 mm in-plane resolution; 1,800 time points). Thirty minutes after radiotracer injection, either PL or 0.25 mg/kg of MP was manually injected intravenously as a ~30-s bolus. During the 90-min PET-fMRI scan, participants were instructed to relax with their eyes open and remain as still as possible. PET image reconstruction and MR image preprocessing can be found in *SI Appendix*.

PET Analysis. We used the SUVr method to evaluate apparent dynamic increases in DA levels (26) which approximates the simplified reference region model (LSSRM). However, the LSSRM approach, although requiring only one scan session, hindered reliable quantification of DA in our data due to five fit parameters and the absence of continuous [^{11}C]raclopride infusion. Nevertheless, our design included a placebo scan for each participant, allowing us to develop an approach that leverages the reliability of placebo scans and overcomes the lack of continuous infusion. This approach, called ΔSUVr, only requires the amplitude and time-to-peak of its derivative for fitting the data, resulting in improved reliability for estimating dynamic "dopamine increases" compared to previous methods.

Functional Connectivity Dynamics. All confounding timeseries calculated by fMRIPrep were regressed out from the individual CIFTI time series with N = 91,282 grayordinates and 1,800 time points using linear regression. ALFF and gFCD timeseries were calculated to assess the dynamics of the spontaneous signal fluctuations and degree of the functional connectivity in the 0.01 to 0.1Hz frequency band. We utilized whole-brain sliding window analysis to examine the dynamics of specific metrics throughout the scan at a temporal resolution of 1 min. The analysis was performed using the Biowulf cluster (https://hpc.nih.gov/), a high-performance computing system. In this study, we employed a fixed rectangular time window with N = 100 fMRI time points (equivalent to 5 min) to ensure the reproducibility of connectivity metrics. This process involved computing dynamic time series comprising 85 time windows. To generate the dynamic time series, we initially calculated the first ALFF and gFCD maps using the data points within the first time window. Then, we shifted the time window by 20 time points (equivalent to 1 min) and recalculated the ALFF and gFCD maps. This shifting and recalculation process was repeated 84 times until all fMRI time points were utilized for mapping the dynamics of ALFF and gFCD. For mapping the gFCD, we employed a correlation threshold of $R > 0.6$. The dynamics of the ALFF and gFCD (24) were assessed using Matlab R2017b (MathWorks, Natick, MA).

Neurovascular Coupling. Multiple linear regression analyses were carried in Matlab to map the slopes of the linear associations of the dependent variable Y [ALFF($\boldsymbol{x}$, t) or gFCD($\boldsymbol{x}$, t)] with the explanatory variables $F(t)$ and $f(t)$,

$$Y(\boldsymbol{x}, t) \sim \beta_1(\boldsymbol{x})F(t) + \beta_2(\boldsymbol{x})f(t), \quad [1]$$

as a function of 85 time windows for each PET/fMRI run.

Group-level statistical analysis. A linear mixed-effects model was employed to assess the statistical significance of neurovascular coupling, represented by β_1 and β_2, across participants. These parameters denote the slopes of the associations between $F(t)$ and $f(t)$ with ALFF(t) and gFCD(t). The analysis was conducted within a whole-brain mask and further explored within 360 cortical partitions, 19 subcortical partitions obtained from Freesurfer, as well as and 12 resting-state networks (34). Linear mixed-effects modeling was also used to assess the relationship between the cardiovascular measures (heart rate, and systolic and diastolic blood pressure) and several predictors (F, f, and drug condition). To determine the statistical significance of the fixed effects, we used a likelihood ratio test comparing the full model to a reduced model without the predictors of interest. The "lmer" function in the "lme4" R-package was utilized to perform these analyses. Additionally, a vertex-wise t test was conducted in Matlab to determine the statistical significance of β_1 and β_2 across participants, independently for IV-MP, oral-MP, and PL conditions. Statistical significance was defined as $P < 0.05$, with multiple comparisons corrected using a FDR correction.

Data, Materials, and Software Availability. All data needed to evaluate the conclusions in the paper are present in the paper and/or *SI Appendix*. The Matlab code and the data supporting the findings of this study are available on figshare.com under the Digital Object Identifier (DOI) (56).

ACKNOWLEDGMENTS. This work was accomplished with the support from the National Institute of Alcohol Abuse and Alcoholism (ZIAAA000550).

Author affiliations: [a]Laboratory of Neuroimaging (LNI), National Institute on Alcohol Abuse and Alcoholism, NIH, Bethesda, MD 20892

1. S. Raman *et al.*, Trends in attention-deficit hyperactivity disorder medication use: A retrospective observational study using population-based databases. *Lancet Psychiatry* **5**, 824–835 (2018).
2. S. McCabe *et al.*, Is age of onset and duration of stimulant therapy for ADHD associated with cocaine, methamphetamine, and prescription stimulant misuse? *J. Child Psychol. Psychiatry*, 10.1111/jcpp.13807 (2023).
3. S. Lakhan, A. Kirchgessner, Prescription stimulants in individuals with and without attention deficit hyperactivity disorder: Misuse, cognitive impact, and adverse effects. *Brain Behav.* **2**, 661–677 (2012).
4. N. Volkow, J. Swanson, Variables that affect the clinical use and abuse of methylphenidate in the treatment of ADHD. *Am. J. Psychiatry* **160**, 1909–1918 (2003).
5. H. Hart, J. Radua, T. Nakao, D. Mataix-Cols, K. Rubia, Meta-analysis of functional magnetic resonance imaging studies of inhibition and attention in attention-deficit/hyperactivity disorder exploring task-specific, stimulant medication, and age effects. *JAMA Psychiatry* **70**, 2 (2013).
6. C. Li, R. Sinha, Inhibitory control and emotional stress regulation: Neuroimaging evidence for frontal-limbic dysfunction in psycho-stimulant addiction. *Neurosci. Biobehav. Rev.* **32**, 581–597 (2008).
7. A. Konova, S. Moeller, D. Tomasi, R. Goldstein, Effects of chronic and acute stimulants on brain functional connectivity hubs. *Brain Res.* **1628**, 147–156 (2015).
8. V. Pereira-Sanchez *et al.*, Resting-state fMRI to identify the brain correlates of treatment response to medications in children and adolescents with attention-deficit/hyperactivity disorder: Lessons from the CUNMET study. *Front. Psychiatry* **12**, 759696 (2021).

9. R. Cary *et al.*, Network structure among brain systems in adult ADHD is uniquely modified by stimulant administration. *Cereb. Cortex* **27**, 3970–3979 (2017).
10. M. Ulrich, K. Heckel, M. Kölle, G. Grön, Methylphenidate differentially affects intrinsic functional connectivity of the salience network in adult ADHD treatment responders and non-responders. *Biol. Basel* **11**, 1320 (2022).
11. A. Kaiser *et al.*, Effects of a single-dose methylphenidate challenge on resting-state functional connectivity in stimulant-treatment naive children and adults with ADHD. *Hum. Brain Mapp.* **43**, 4664–4675 (2022).
12. K. Griffiths *et al.*, Understanding the neural mechanisms of lisdexamfetamine dimesylate (LDX) pharmacotherapy in Binge Eating Disorder (BED): A study protocol. *J. Eat. Disord.* **7**, 23 (2019).
13. H. Yang *et al.*, Amplitude of low frequency fluctuation within visual areas revealed by resting-state functional MRI. *Neuroimage* **36**, 144–152 (2007).
14. J. Yoo, D. Kim, J. Choi, B. Jeong, Treatment effect of methylphenidate on intrinsic functional brain network in medication-na < ve ADHD children: A multivariate analysis. *Brain Imag. Behav.* **12**, 518–531 (2018).
15. Y. Zang *et al.*, Altered baseline brain activity in children with ADHD revealed by resting-state functional MRI. *Brain Dev.* **29**, 83–91 (2007).
16. B. Biswal, F. Yetkin, V. Haughton, J. Hyde, Functional connectivity in the motor cortex of resting human brain using echo-planar MRI. *Magn. Reson. Med.* **34**, 537–541 (1995).
17. R. Birn *et al.*, Changes in endogenous dopamine induced by methylphenidate predict functional connectivity in nonhuman primates. *J. Neurosci.* **39**, 1436–1444 (2019).
18. X. Di *et al.*, The influence of the amplitude of low-frequency fluctuations on resting-state functional connectivity. *Front. Hum. Neurosci.* **7**, 118 (2013).
19. D. Tomasi, N. Volkow, Association between brain activation and functional connectivity. *Cereb. Cortex* **29**, 1984–1996 (2019).
20. M. Judenhofer *et al.*, Simultaneous PET-MRI: A new approach for functional and morphological imaging. *Nat. Med.* **14**, 459–465 (2008).
21. S. Kim *et al.*, Cerebral blood volume MRI with intravascular superparamagnetic iron oxide nanoparticles. *NMR Biomed.* **26**, 949–962 (2013).
22. C. Sander *et al.*, Neurovascular coupling to D2/D3 dopamine receptor occupancy using simultaneous PET/functional MRI. *Proc. Natl. Acad. Sci. U.S.A.* **110**, 11169–11174 (2013).
23. C. Sander, J. Hooker, C. Catana, B. Rosen, J. Mandeville, Imaging agonist-induced D2/D3 receptor desensitization and internalization in vivo with PET/fMRI. *Neuropsychopharmacology* **41**, 1427–1436 (2016).
24. D. Tomasi, N. Volkow, Functional connectivity density mapping. *Proc. Natl. Acad. Sci. U.S.A.* **107**, 9885–9890 (2010).
25. D. Tomasi, G. Wang, N. Volkow, Energetic cost of brain functional connectivity. *Proc. Natl. Acad. Sci. U.S.A.* **110**, 13642–13647 (2013).
26. D. Tomasi *et al.*, Time-varying SUVr reflects the dynamics of dopamine increases during methylphenidate challenges in humans. *Commun. Biol.* **6**, 166 (2023).
27. N. Volkow *et al.*, Dopamine transporter occupancies in the human brain induced by therapeutic doses of oral methylphenidate. *Am. J. Psychiatry* **155**, 1325–1331 (1998).
28. N. Volkow *et al.*, Imaging endogenous dopamine competition with [11C]raclopride in the human brain. *Synapse* **16**, 255–262 (1994).
29. J. Swanson, N. Volkow, Pharmacokinetic and pharmacodynamic properties of stimulants: Implications for the design of new treatments for ADHD. *Behav. Brain Res.* **130**, 73–78 (2002).
30. J. Logan *et al.*, Distribution volume ratios without blood sampling from graphical analysis of PET data. *J. Cereb. Blood Flow Metab.* **16**, 834–840 (1996).
31. N. Volkow *et al.*, Relationship between blockade of dopamine transporters by oral methylphenidate and the increases in extracellular dopamine: Therapeutic implications. *Synapse* **43**, 181–187 (2002).
32. Z. Luo, N. Volkow, N. Heintz, Y. Pan, C. Du, Acute cocaine induces fast activation of D1 receptor and progressive deactivation of D2 receptor striatal neurons: In vivo optical microprobe [Ca2+]i imaging *J. Neurosci.* **31**, 13180–13190 (2011).
33. J. Choi, Y. Chen, E. Hamel, B. Jenkins, Brain hemodynamic changes mediated by dopamine receptors: Role of the cerebral microvasculature in dopamine-mediated neurovascular coupling. *Neuroimage* **30**, 700–712 (2006).
34. J. Ji *et al.*, Mapping the human brain's cortical-subcortical functional network organization. *Neuroimage* **185**, 35–57 (2019).
35. J. Wisor *et al.*, Dopaminergic role in stimulant-induced wakefulness. *J. Neurosci.* **21**, 1787–1794 (2001).
36. N. Fultz *et al.*, Coupled electrophysiological, hemodynamic, and cerebrospinal fluid oscillations in human sleep. *Science* **366**, 628–631 (2019).
37. C. Chang *et al.*, Tracking brain arousal fluctuations with fMRI. *Proc. Natl. Acad. Sci. U.S.A.* **113**, 4518–4523 (2016).
38. C. Orban, R. Kong, J. Li, M. Chee, B. Yeo, Time of day is associated with paradoxical reductions in global signal fluctuation and functional connectivity. *PLoS Biol.* **18**, e3000602 (2020).
39. N. Volkow *et al.*, Effects of expectation on the brain metabolic responses to methylphenidate and to its placebo in non-drug abusing subjects. *Neuroimage* **32**, 1782–1792 (2006).
40. S. Halani, J. Kwinta, A. Golestani, Y. Khatamian, J. Chen, Comparing cerebrovascular reactivity measured using BOLD and cerebral blood flow MRI: The effect of basal vascular tension on vasodilatory and vasoconstrictive reactivity. *Neuroimage* **110**, 110–123 (2015).
41. W. Chen, P. Liu, N. Volkow, Y. Pan, C. Du, Cocaine attenuates blood flow but not neuronal responses to stimulation while preserving neurovascular coupling for resting brain activity. *Mol. Psychiatry* **21**, 1408–1416 (2016).
42. N. Volkow *et al.*, Is methylphenidate like cocaine? Studies on their pharmacokinetics and distribution in the human brain. *Arch. Gen. Psychiatry* **52**, 456–463 (1995).
43. Y. Liu *et al.*, Cocaine's cerebrovascular vasoconstriction is associated with astrocytic Ca2+ increase in mice. *Commun. Biol.* **5**, 936 (2022).
44. J. Pinto, M. Bright, D. Bulte, P. Figueiredo, Cerebrovascular reactivity mapping without gas challenges: A methodological guide. *Front. Physiol.* **11**, 608475 (2021).
45. B. Biswal, A. Hudetz, F. Yetkin, V. Haughton, J. Hyde, Hypercapnia reversibly suppresses low-frequency fluctuations in the human motor cortex during rest using echo-planar MRI. *J. Cereb. Blood Flow Metab.* **17**, 301–308 (1997).
46. X. Hou *et al.*, Estimation of brain functional connectivity from hypercapnia BOLD MRI data: Validation in a lifespan cohort of 170 subjects. *Neuroimage* **186**, 455–463 (2019).
47. S. Lohani, A. Poplawsky, S.-G. Kim, B. Moghaddam, Unexpected global impact of VTA dopamine neuron activation as measured by opto-fMRI. *Mol. Psychiatry* **22**, 585–594 (2017).
48. H. Decot *et al.*, Coordination of brain-wide activity dynamics by dopaminergic neurons. *Neuropsychopharmacology* **42**, 615–627 (2017).
49. R. McCutcheon *et al.*, Mesolimbic dopamine function is related to salience network connectivity: An integrative positron emission tomography and magnetic resonance study. *Biol. Psychiatry* **85**, 368–378 (2019).
50. R. McCutcheon *et al.*, Dopaminergic organization of striatum is linked to cortical activity and brain expression of genes associated with psychiatric illness. *Sci. Adv.* **7**, eabg1512 (2021).
51. D. Cole *et al.*, Differential and distributed effects of dopamine neuromodulations on resting-state network connectivity. *Neuroimage* **78**, 59–67 (2013).
52. D. Tomasi, E. Shokri-Kojori, N. Volkow, Temporal changes in local functional connectivity density reflect the temporal variability of the amplitude of low frequency fluctuations in gray matter. *PLoS One* **11**, e0154407 (2016).
53. G. J. Wang *et al.*, Methylphenidate decreases regional cerebral blood flow in normal human subjects. *Life Sci.* **54**, PL143–PL146 (1994).
54. Ş Demiral *et al.*, Methylphenidate's effects on thalamic metabolism and functional connectivity in cannabis abusers and healthy controls. *Neuropsychopharmacology* **44**, 1389–1397 (2019).
55. N. Volkow *et al.*, Cardiovascular effects of methylphenidate in humans are associated with increases of dopamine in brain and of epinephrine in plasma. *Psychopharmacology (Berl)* **166**, 264–270 (2003).
56. D. Tomasi, *et al.*, Tabulated PET-fMRI data corresponding to "Examining the Role of Dopamine in Methylphenidate's Effects on Resting *Brain* Function". Figshare. https://figshare.com/articles/dataset/shared_data_zip/24769032. Deposited 8 December 2023.